Material Testing Device Using Magnetic Levitation Mechanism

Koichi OKA [a], Mengyi REN [a]

a Kochi University of Technology, Miyanokuchi 185, Tosayamada-cho, Kami, Kochi, Japan (oka.koichi@kochi-tech.ac.jp)

Abstract

This paper describes non-contact material testing devices using magnetic levitation mechanism, in which a specimen can be tested in tension, compression, bending or torsion while the specimen and few parts are being levitated. We mainly focus on the mechanism, control, and experimental results of the tension testing device and bending testing device. The structures of these devices are introduced about material testing methods. For material testing, additional control mechanisms are required except for ordinal levitation control mechanism. Tension testing device and bending testing device have corresponding mechanism respectively. Experimental examinations were performed to examine the feasibility, stability, and robustness under the maxim tension force and bending force. Finally, they demonstrated that the levitation control system has good stability and robustness under the maximum tension force and bending force.

Keywords: *Material testing device, Non-contact testing device, Tension test, Bending test.*

1. Introduction

Magnetic levitation has been widely studied and applied in many industrial applications due to the advantage of non-contact, e.g., high-speed bearings (Supreeth, et al, 2022), (Prrasad, et al, 2021), motors (Kumashiro, at al, 2022), (Wang, at al, 2023), and centrifugal blood pumps (Masuzawa, at al, 2000), (Wu, at al, 2021), etc. As a new application of magnetic suspension system, Tada (2013) has been proposed the magnetic force for the material testing device(MTD). This testing device is easily used for the special liquid environment test. However as this device has an mechanical contact at one end of specimen hold mechanism, if the test in the vacuum environments are required the whole equipment of testing device should be inside a large vacuum chamber. A more sensible approach is to apply a non-contact force from the outside of the vacuum chamber to the specimen inside the vacuum chamber. Magnetic levitation (maglev) technology makes this possible.

In this paper, a mag-lev testing devices, where the specimen can be pulled in a non-contact way, are discussed. We develop a perfect non-contact MTD for compact testing device. As the development of MTD, a tension test device and bending test device are introduced in this paper. This application will bring benefits, because some materials' working environments are special, such as high-purity aluminum (Wan et al,2022), gas-lubricated bearings (Kumar at al, 2022). and S-Glass-Carbon fiber reinforced polymer composites (Elango, et al, 2021). Previously, if we want to test these materials, we have to place a whole testing device including framework, force sensor and actuator, etc. in a container where the special environment can be created. However, some parts of the testing device, e.g., circuits in the force sensor and actuator are sensitive to environmental factors such as temperature, air pressure, humidity, etc. With magnetic levitation, only few parts and specimen need to be put in the container, which greatly increases the feasibility of the tests. The structure of this paper is given as follows. Chapter II presents a structure and experimental results of a tension testing device; Chapter III describes a structure, control method, and experimental results of a 3 point bending testing device working in MLMMTD (magnetic levitation mechanism material testing device).

2. Material tension testing device

2.1 Overall structure

The initial structure of MTD is shown in Figure 1. As shown in the figure, two electromagnets (EM), called top EMs, were fixed at the top of the framework, and one EM, called bottom EM, was fixed at the bottom of the framework by a load cell. The currents of the three EMs were controlled individually by three controllers. The levitated object is in the middle of MTD as shown to the right in the figure, and it includes two top floaters, two top fixtures, two bottom fixtures and one bottom floater. The two ends of the specimen were placed in the slit of the top and bottom fixtures respectively.

The working principle of MTD is, firstly, the two top EMs, whose currents are controlled individually, attract the two top floaters respectively. The two eddy current sensors feed the position of the two top floaters to a controller, which then adjusts the currents of the two top EMs to maintain the top floaters and the fixtures in a constant vertical position. Subsequently, the bottom EM is electrified, and generates a tension force on the bottom floaters, and the current of

the bottom EM gradually increases while the top floaters and the fixtures maintain in the original position until the specimen is destroyed. The load cell measures the tension force for recording, and also for control feedback.

The levitation of the two top floaters are controlled by the two top EMs, this may be easy. However, after tension force is loaded, to maintain the levitation, it is necessary to consider suppressing the disturbance caused by the tension force. A material mechanics testing device needs to measure both loading force and specimen elongation to obtain stress-strain curve. In MTD, the load cell can indirectly measure the loading force. The elongation is equal to the amount of change in the bottom air gap. Moreover, the bottom air gap can be calculated according to equation, which describes the magnetic force of an electromagnet.

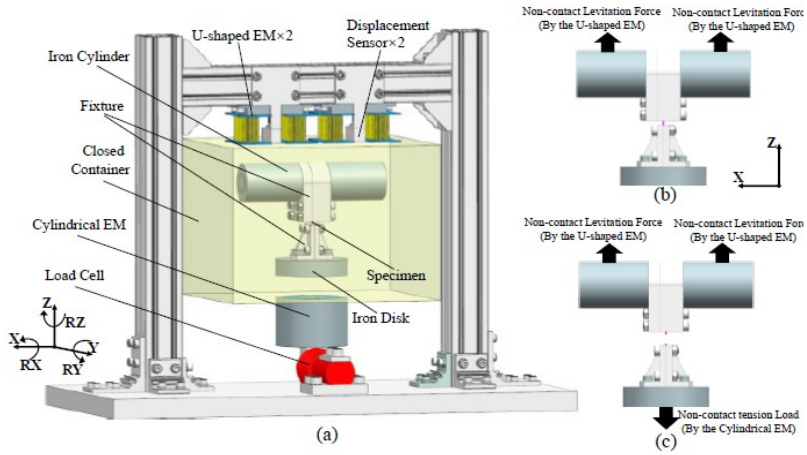

Figure 1 Conceptual illustration of proposed tension test device using magnetic suspension mechanism

2.2 Control system and experimental results

When there is no tension force, the function of the controller is very simple. However, tension force applied to the lower floater will form a disturbance on the system, and it is necessary to compensate. Because the maglev system has large non linearity. In the process of applying tension force, the currents of the top EMs will continuously increase to maintain the levitation, so the plant model will inevitably deviate away from the original plant model. In other words, as the currents of the top EMs increase continuously, the inherent non-linearity of the magnetic levitation system will appear, the constant force feedback gains will no longer fit the plant model after the deviation. Therefore, an improved method shown in Figure 2 was proposed. Dynamic force feedback gains instead of the constant force feedback gains are used for the control system. In the figure, the dynamic force feedback gains consist of a superpositions of the proportion and integral of air gap errors. In addition, the precise tension feedback path in Figure 3 was employed to compensate for the deviation caused by changes in the lower air gap. With such a control system, the tension force was gradually applied at a fixed rate to the bottom EM.

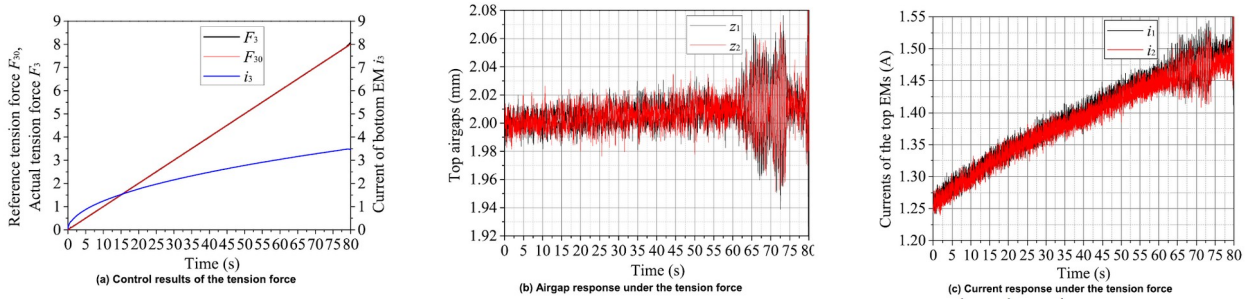

Figure 2 Experimental result of tension test

3. 3 point bending test device

3.1 Overall structure

As shown in Figure 3, the prototype mainly consists of two U-shaped electromagnets, two eddy current sensors, levitated object, a cylindrical electromagnet, and a force sensor. The two U-shaped electromagnets are used to produce levitation force for the levitated object, while the two eddy current sensors are used to determine the position of the two iron cylinders. The cylindrical electromagnet is used to produce a non-contact bending load to bent the specimen in the levitated object, while the force sensor is used to measure the bending load in real time.

The principle is, as shown in Figure 4, firstly, the two U-shaped electromagnets and the two eddy current sensors work to maintain the levitation. The levitation forces will keep the levitated object in a fixed vertical position. As shown in the lower of Figure 4, after the levitation is stable, the cylindrical electromagnet will be energized to produce a non-contact bending load to the iron disk, so that the punch will be pulled down to bend the specimen.

In addition, the applicable maximum deflection of MLBTD is 10mm, which is obtained according to the stroke of the punch component. The applicable maximum bending force of MLBTD is 50N, which is obtained according to the measuring range of the load cell. The applicable specimen stiffness range of MLBTD is more than 430N/m, which is calculated according to the stroke and weight of the punch component, because under the weight of the punch component, too soft specimens will be bent to the maximum deflection before the bending force is applied, so the applicable specimen stiffness has a lower limit. The accuracy of the eddy current sensor is 0.002mm. The accuracy of the load cell is 0.005N.

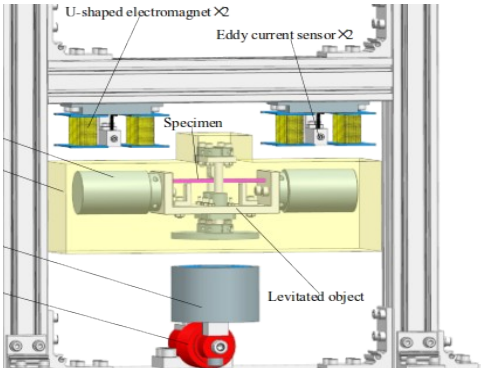

Figure 3 An illustration of 3 point bending testing device

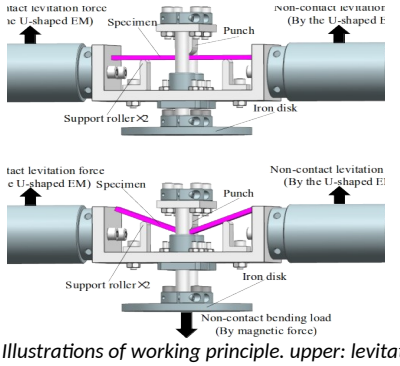

Figure 4 Illustrations of working principle. upper: levitation, lower:applying bending force.

3.2 System modeling

The first step in designing a controller is to get a plant model. Therefore, a state space model for the levitation plant was built as follows. Figure 5 shows an illustration of the levitation plant model. As shown in Figure, i_1 and i_2 denote the currents of the two U-shaped EMs respectively. z_1 and z_2 denote the air gaps between the two U-shaped EMs and the two iron cylinders respectively. F_1 and F_2 denote the attractive force of the two U-shaped EMs to the two iron cylinders. F_b denotes the bending force, which comes from the cylindrical EM and acts to the iron disk. mg denotes the weight of the levitated object. In this model, Both F_b and mg were assumed to always act to the center of mass (COM) of the levitated object. z_M denotes the vertical distance from the COM to the lower surface of the U-shaped EM. θ denotes the tilting angle of the iron cylinders. It was assumed that both the position of the COM and the moment of inertia (MOI) of the levitated object around the COM were invariant even if the punch move.

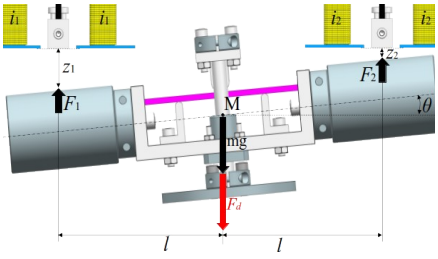

Figure 5 An illustration for levitation plant model

To get a mathematical model, firstly, both F_1 and F_2 were linearized at a working point (i_0, z_0) as follows.

$$\begin{cases} F_1 = F_{1(i_0,z_0)} + k_i(i_1 - i_0) - k_z(z_1 - z_0) \\ F_2 = F_{2(i_0,z_0)} + k_i(i_2 - i_0) - k_z(z_2 - z_0) \end{cases} \quad (1)$$

Where, $F_{1(i0,\ z0)}=F_{2(i0,\ z0)}=(mg+F_b)/2$, k_i and K_z are the current coefficient and displacement coefficient of a single U-shaped EM respectively. The dynamics of the levitated object is described as follows.

$$mg - (F_1 + F_2) = m\ddot{z}_M,\ (F_2 - F_1)l = J\ddot{\theta} \quad (2)$$

where, m is the mass of the levitated object; J is the moment of inertia of the levitated object around the COM. According to the geometric relationship, z_M is equal to $(z_1+z_2)/2$. In addition, assuming that θ is extremely small, θ can be considered to be equal to $(z_1-z_2)/2l$. Furthermore, defining $\Delta z_+=z_1+z_2$, $\Delta z_-=z_1-z_2$, $\Delta i_+=i_1+i_2$, $\Delta i_-=i_1-i_2$, and substituting Eq (1) into Eq (2), Two differential equations can be obtained as follows.

$$m\Delta\ddot{z}_{+} = -2k_i\Delta i_{+} + 2k_z\Delta z_{+},\ J\Delta z_{-} = -2k_i l^2\Delta i_{-} + 2k_z l^2\Delta z_{-} \tag{3}$$

Then, two transfer functions can be derived from Eq (3) as follows.

$$\frac{\Delta z_{+}}{\Delta i_{+}} = \frac{-2k_i}{ms^2 - 2k_z},\ \frac{\Delta z_{-}}{\Delta i_{-}} = \frac{-2k_i l^2}{Js^2 - 2k_z l^2} \tag{4}$$

where, Δi_{+} and Δi_{-} are the inputs of the systems, Δz_{1+} and Δz_{-} are the outputs of the systems. The transfer functions reflect the dynamic characteristics of Z DOF and RY DOF respectively.

3.3 Fixed stiffness-damping control of levitation

When the bending force is applied, the levitated object will be in a state of alternating pulling up and down, which poses high requirement on the levitation stiffness. Therefore, the higher the levitation stiffness, the better. However, for a certain hardware, the levitation stiffness that it can hold is limited due to noise and time delay. If we use a traditional PID-controller, with the increase of the bending force, the integrator will increase current to compensate for the bending force, as a result, the levitation stiffness will change. No matter the levitation stiffness increases or decreases, it cannot remain at a fixed value, which means the highest levitation stiffness can only exist for a moment. This will bring some negative effect, for example, if we tune the PD-gains to get the highest levitation stiffness at the beginning, after the bending force increases, the levitation stiffness may exceed the highest value, which will beyond hardware's tolerance and cause instability. On the contrary, the levitation stiffness may also decrease with the increasing of the bending force, which may result in insufficient levitation stiffness to resist the bending force. Therefore, a better solution is keeping the levitation stiffness at the highest value all the time. In addition, the role of levitation damping is to suppress oscillation caused by levitation stiffness, therefore, it is better to keep the levitation damping constant to match the constant levitation stiffness. Given the above discussion, a fixed stiffness-damping (FSD) control was employed, which avoids the risk of insufficient levitation stiffness and levitation stiffness exceeding the upper limit. FSD is also realized based on PD-controller, the difference is, the PD-gains of FSD are scheduled according to a certain rule. The block diagram of the FSD control is shown in Figure 6.

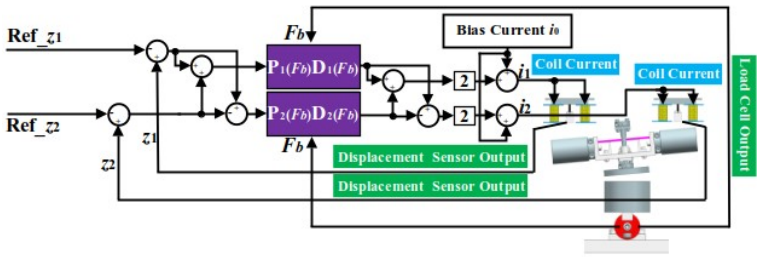

Figure 6 Block diagram of fixed stiffness and damping control system

3.4 Control of the bending force

As shown in Figure 7(a) F_b is the bending force, it is the attractive force of the cylindrical EM to the iron disk. As shown in Figure 7(b), the dynamics of a three-point bending specimen can be regarded as a mass-spring-damper system, where K_S and C_S are the stiffness and viscous damping of the specimen respectively. As l_S is the deflection of the specimen and z_3 is the bottom air gap, the value of z_3+l_S is identified. Therefore, the linearized dynamics model is

$$m_b\ddot{l}_S + C_S\dot{l}_S + (K_S - k_{bz})l_s = k_{bi}i_b \tag{5}$$

where, k_{bz} and k_{bi} is the displacement and current coefficients of the electromagnet.

Our goal is to enable the device to apply ramp forces smoothly over a wide range of materials. For this purpose, as shown in Figure 8, a force control system was designed, and a PI-controller was employed in the force control system because there is a nearly identical case(Ishizaki, at el, 2010) that shown that it is feasible to use PI-controller.

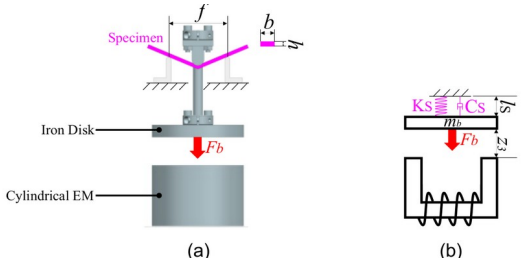

Figure 7 An illustration of bending model

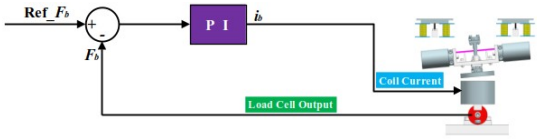

Figure 8 Bending force control system

3.5 Experiment

An experiment was performed to verify the feasibility of the special configuration and FSD control method and to verify the feasibility of the force control system. Figure 9 presents a photograph of the experiment platform.

The experiment was conducted with the identical FSD-controllers and a low-stiffness specimen to test the force control system shown in Figure 8. This is because soft materials will have high deformation and pose high requirement on the force control system, which can test the force control system for good or bad. The specification of the specimen is shown in Table. 1.

Table 1 Specification of material of specimen

Material	*Length*	*Width*	*Height*	*Elastic Modulus*	*Yield Strength*
Z-ABS	86 mm	8 mm	3.7 mm	1080 MPa	30.3 MPa

As shown in Figure 10(a), the air gaps were relatively stable over the 24s. As shown in Figure 10(c), the loading of F_b was relatively stable and smooth over the 24s though there is a little error between the reference input and the actual force in the first 2s; but there had a little oscillation on the F_b curve between 21s and 24s, this is because the iron disk almost had contact with the cylindrical EM due to the large deflection of the specimen; At about 24s, the levitated object fell down, because the iron disk was completely sucked by the cylindrical EM. Overall, the loading process was fairly smooth, the F_b curve can still maintain a slope shape even when the iron disk was extremely close to the cylindrical EM. Therefore, it can be concluded that the force control system is feasible under large deflection.

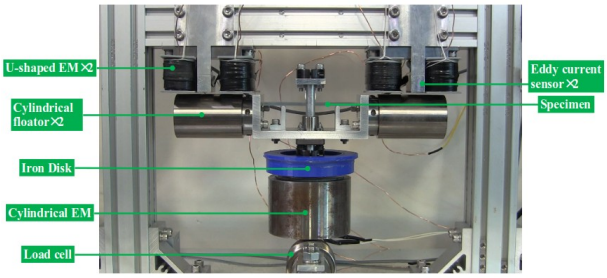

Figure 9 Experimental setup for examination

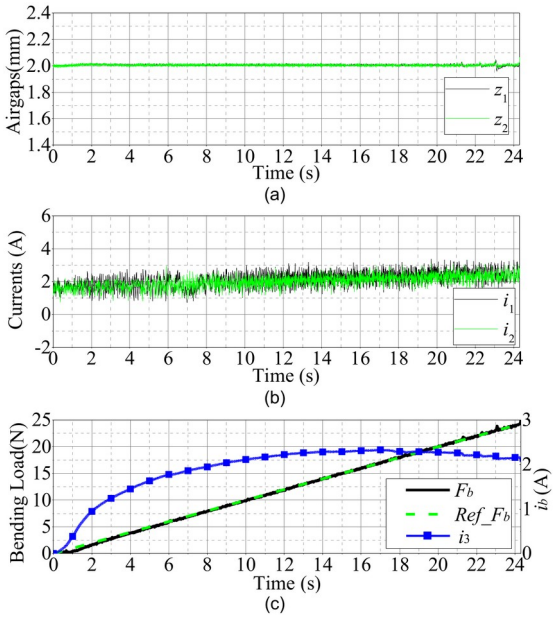

Figure 10 Experimental result with force control system (a) air gap response, (b) current, (c) force control result

4. Conclusion

This paper presents a non-contact tension and bending testing device using magnetic levitation technology, which is expected to be applied to material testing in special environments. Experiment demonstrated that this structure can guarantee the passive stability of the four DOFs. In addition, a fixed stiffness-damping (FSD) controller was designed to maintain the levitation under the bending force, and a force control system was designed to control the loading of the bending force. The experiment result with the bending test device demonstrated that the force control system allows the device to load the bending force smoothly even under large deflection. It can be seen from the experiments, the air gap oscillation amplitudes with different materials were different, and air gap oscillation amplitude influences test accuracy. Therefore, the dependence of test accuracy on specimen stiffness is worth to be investigated in our future work.

References

Journal article

D. K. Supreeth, S. I. Bekinal, S. R. Chandranna and M. Doddamani, “A Review of Superconducting Magnetic Bearings and Their Application,” IEEE Trans. Appl. Supercond., vol. 32, no. 3, pp. 1-15, Apr. 2022.

K. N. V. Prasad and G. Narayanan, “Electromagnetic Bearings With Power Electronic Control for High-Speed Rotating Machines: Review, Analysis, and Design Example,” IEEE Trans. Ind. Appl., vol. 57, no. 5, pp. 4946-4957, Sept.-Oct. 2021.

X, Wang, et al. “Study on the Effect of Suspension Windings on the Electromagnetic Vibration and Noise of Ultra-high-Speed Bearingless Permanent Magnet Synchronous Motor for Air Compressor,” IEEJ Trans. Electr. Electron. Eng., vol. 18, no. 1, pp. 129-138, Sept. 2023.

T. Masuzawa, S. Ezoe, T. Kato, Y. Okada, "Magnetically Suspended Centrifugal Blood Pump with an Axially Levitated Motor", Artificial Organs, vol. 4, issue6, pp. 468-474, June 2000

P. Wu, et al. “On the optimization of a centrifugal maglev blood pump through design variations,” Front. Physiol., vol. 12, pp. 699891, June 2021

H. Wan, et al., “Zone melting under vacuum purification method for high-purity aluminum,” Journal of Materials Research and Technology, vol. 17, pp. 802-808, Jan. 2022.

C. Kumar and S. Sarangi, “Dynamic behavior of self-acting gas-lubricated long journal bearing,” Mechanics Research Communications, vol. 124, pp. 103950, Aug. 2022.

Natarajan, Elango, et al. “Experimental and numerical analysis on suitability of S-Glass-Carbon fiber reinforced polymer composites for submarine hull,” Defense Technology, vol. 19, pp. 1-11, Jan. 2023.

Conference article

A. Kumashiro, A. Chiba, W. Gruber, W. Amrhein and G. Jungmayr, “Novel Reluctance-type Magnetic Geared Motor with Integrated with High-speed Bearingless Motor,” 2022 Int. Conf. Power Electron. (IPEC-Himeji 2022- ECCE Asia), Himeji, Japan, 2022, pp. 1762-1768.

N. Tada and H. Masago, "Remotely-controlled tensile test of coppercored lead-free solder joint in liquid using permanent magnet," 2013 8th International Microsystems, Packaging, Assembly and Circuits Technology Conference (IMPACT), 2013, pp. 186-189.

N. Tada and T. Uemori, “Time-dependent fracture of copper-cored lead-free solder ball and nickel rod joints in air, distilled water, and NaCl solution,” in Proc. International Microsystems, Packaging, Assembly and Circuits Technology Conference, Oct. 2017, pp. 168-171.

Ishizaki, Takayuki, et al., “PI control system design for Electromagnetic Molding Machine based on Linear Programing,” in Proc. IEEE International Conference on Control Applications, Sep. 2010, pp. 2415-2420